Multiscale Modeling of Electromagnetic Telemetry in Layered Transverse Isotropic Formation

Shubin Zeng, *Student Member, IEEE*, Donald R. Wilton, *Life Fellow, IEEE*, and Jiefu Chen, *Member, IEEE*

***Abstract*—Electromagnetic telemetry (EMT) systems are utilized for measurement while drilling to transmit data from borehole to the ground surface during drilling or vice versa. To help predict the successful deployment of the EMT system within complex formation and environmental noise, a reliable numerical algorithm is developed and applied to model the EMT system for directional drilling in layered transverse isotropic (TI) formation. In the telemetry system, the long and thin drill string having three-dimensional trajectory acts as an underground antenna that can be modeled as a thin wire excited by a delta gap voltage/current source near the drill bit. Using the thin wire assumption, the developed algorithm calculates the thin wire kernel in homogeneous uniaxial media with high accuracy to reduce the dimension and complexity of the problem. The mixed-potential form of layered media Green's function and electric field integral equation are used to model the electromagnetic interaction of the drill string and layered TI media. The effect of drilling fluid outside the pipe is modeled using the volumetric equivalence principle. The accuracy and efficiency of the new algorithm are demonstrated by several numerical examples.**

***Index Terms*—Electric field integral equation (EFIE), electromagnetic telemetry (EMT), layered media Green's function (LMGF), method of moments (MoM), thin wire kernel.**

I. Introduction

DRILLING is a core area of the oil and gas upstream energy business. Drilling-related activities take up to 60% of the entire exploration budget of oilfield wells [1]. Drilling is also essential to many other areas, such as geothermal exploration, CO2 sequestration, nuclear waste disposal, etc. While drilling, a variety of measurements, such as temperature, pressure, resistivity logging, nuclear logging, etc., are acquired in the borehole environments, and then sent to the surface to ensure safety, to adjust the well trajectory on the fly to reach the geological targets, and to keep the wellbore within a desired formation. The process of sending downhole measurements to the surface, or sending drilling commands from the surface to downhole tools, is called telemetry. Because no cable can be deployed in the borehole during drilling, borehole telemetry in oilfield drilling is achieved by wireless communication.

Manuscript received August 14, 2018; revised October 31, 2018; accepted December 5, 2018. Date of publication December 28, 2018; date of current version January 18, 2019. This work was supported by the Funding for Advanced Computing (SeFAC), Core facility for Advanced Computing and Data Systems (CACDS), University of Houston. *(Corresponding author: Jiefu Chen.)*

The authors are with the Department of Electrical and Computer Engineering, University of Houston, Houston, TX 77004 USA (e-mail: szeng4@uh.edu; dwilton@mindspring.com; jchen84@uh.edu).

Digital Object Identifier 10.1109/JMMCT.2018.2890071

There exist two such borehole communication technologies: mud pulse telemetry (MPT) and electromagnetic telemetry (EMT). For MPT, a downhole valve is operated to restrict the flow of drilling mud and to create pressure pulse carrying digital information and propagating to the surface. MPT is a mature and widely used downhole communication technique, but it has severe limitations: It involves moving parts prone to failure during operation, and it cannot work in underbalanced drilling using air or foam as drilling fluid, or when fluid loss of circulation is encountered [2]. EMT is based on electromagnetic waves propagating in underground formation between downhole tool and the surface. Compared with MPT, EMT has been proven to have better reliability as no moving part is involved during drilling, and it has the potential to provide a much higher rate of data transmission [3]. Since EMT does not rely on the drilling fluid column as a communication channel, EMT systems are preferred in underbalanced drilling jobs (using dust, mist, foam, or air as drilling fluid), or in areas where loss of circulation is prevalent (e.g., inherently fractured formation).

While the MPT signal strength is predominantly determined by drilling depth, the received signal intensity of an EMT system is dependent upon a variety of factors, such as well trajectory, formation structure and conductivity, drilling fluid, operation frequency, and the layout of the surface receiver. Accurate prediction of EMT performance by efficient and robust numerical modeling is critical in justifying the employment of EMT over MPT for a specific job, and it is also essential in maximizing EMT received signals and optimizing for carrier frequency, bandwidth, and battery life as drilling depth increases.

Modeling an EMT system is essential simulation of low-frequency electromagnetic fields propagating through underground formation. One of the greatest challenges of the EMT modeling is to discretize the complicated and multiscale EMT structure: the entire computational domain is on the order of thousands of feet, and such a large volume will include hundreds of or even more formation layers; besides, the drilled borehole including drill string is very long (thousands of feet) and thin (several inches in diameter), and can contain even finer features (e.g., standoff between drill string and borehole wall is a fraction of an inch). Different numerical methods have been proposed and applied to model the EMT system in homogeneous formation [4], [5] or half-space [6]–[8]. Among these methods, the most commonly used method is based on the integral equation (IE) method. The IE method has been used to model both vertical and deviated drill strings with infinite or finite conductivity in homogeneous conductive media and

half-space media. It is well known that the commonly used formation model in geophysics is horizontally layered media, each layer being composed of homogeneous material with isotropic or uniaxial (i.e., transverse isotropic) conductivity. Recently, the modeling of vertical energized casing in layered media was solved by Yang *et al.* [9], who solved the modeling of horizontally layered media by resorting to the boundary conditions of the electromagnetic field at the interfaces of layers. Besides, Wei [10] developed the analytical solution of the current distribution along an arbitrary oriented but straight metal wire antenna by solving the solutions of vertical and horizontal electric dipoles in layered isotropic media. Besides the IE method, other numerical methods that are available for specific EMT systems, such as the finite-element method (FEM) [11] and numerical mode matching method [12], were applied to model vertical wells in layered media. But these methods are not quite suitable for the modeling of the EMT system due to the large number of unknowns resulting from the spatial discretization or its inability to model drill string with three-dimensional (3-D) trajectory.

Even though the IE method is suitable and accurate to model the EMT system, the previous works are insufficient to model the EMT system for directional drilling in layered uniaxial media. The reason comes from three folds. First, it is well known that the earth formation has uniaxial conductivity due to the sedimentary process. Previous methods are limited to the isotropic media, no matter homogeneous or horizontally layered. Second, in directional drilling, the trajectory of the whole well is partly vertical and partly deviated or horizontal. To model such a 3-D trajectory, one needs more considerations and mathematical calculations. Finally, most previous works simplify the drill string as a long perfect electric conductor (PEC) pipe and neglect the drilling fluids filled in the borehole, whereas both rigorous theoretical studies and field jobs suggest that the electrical properties of drill string and drilling fluid can substantially affect the signal strength of an EMT system.

In this paper, we will discuss an efficient IE-based numerical scheme for modeling multiscale EMT systems in layered transverse isotropic formation. To model the electromagnetic field excited by a voltage/current source embedded in a 3-D drill string accurately, the electric filed integral equation (EFIE) [13] is applied to model the electric field on the surface of the drill string. The finite conductivity of the pipe is modeled by surface impedance of a conductive rod [14]. The thin wire kernel [15] is applied to reduce the surface integral on the drill string into a line integral along the axial direction of the drill string, saving a lot of computation costs. The method of moments (MoM) [16] is employed to discretize the 3-D line geometry into straight segments and obtain the system linear equations. To model the electromagnetic interactions between the drill string and surrounding layered uniaxial media, the mixed-potential form of layered media Green's function (MP-LMGF) for uniaxial media [17] is calculated and utilized with singularity extraction scheme. Some preliminary discussion and results for layered isotropic media can be found in [18] and [19]. Besides the conventional EFIE combining with MP-LMGF as developed in this paper, augmented EFIE (A-EFIE) [20] as well as current and charge integral equations [21] combining matrix friendly LMGF also have been applied to analyze low-frequency scattering problem in layered media.

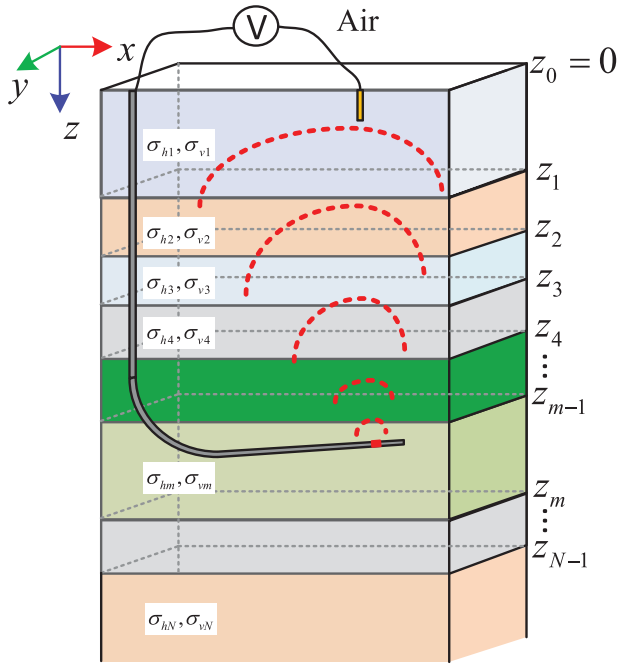

Fig. 1. Schematic of EMT system for directional drilling in layered formation.

The rest of this paper is organized as follows. In Section II, we present the formulation of modeling methods for EMT system. In Section III, we illustrate the performance of the efficient modeling method on solving EMT system in vertical well, horizontal well, vertical well with drilling fluid, and finally a crosswell scenario. Conclusions are given in Section IV.

II. Formulation of Modeling Methods

Fig. 1 shows a schematic of an EMT system for directional drilling in horizontally layered transverse isotropic formation. For the layered media, each layer has horizontal and vertical conductivities $(\sigma_{hi}, \sigma_{vi})$ $(i = 1, 2, \ldots, N)$. A voltage/current source located near the drill bit emits electromagnetic waves into the layered formation. A voltmeter is deployed at the surface to detect the voltage drop between the drill string and one electrode inserted into the ground some distance away. In this paper, the time factor $e^{j\omega t}$ is implied.

A. Thin Wire in Homogeneous Isotropic Media

To model the electromagnetic fields excited by the voltage or current source, we apply the EFIE in the frequency domain

$$\left[\mathbf{E}^i(\mathbf{r}) + \mathbf{E}^s(\mathbf{r})\right]_{\tan} = Z_i \mathbf{I}(\mathbf{r}), \quad \mathbf{r} \in S \tag{1}$$

to represent the total tangential electric field on the surface of the drill string that is represented by S. $\mathbf{I}(\mathbf{r})$ is the total current along the drill string, which is assumed to be axially directed when the drill string is very thin. Z_i denotes the internal impedance of the drill string and characterizes the effect of the finite conductivity of the drill string. If we assume that the drill string is a perfect conductor, then Z_i vanishes. If the conductivity of the drill string

is finite, e.g., σ_d, we can assign a specific value to Z_i as [6]

$$Z_i = \frac{\gamma}{2\pi a\sigma_d}\frac{J_0(\gamma r_e)}{J_1(\gamma r_e)} \tag{2}$$

where $\gamma = \sqrt{\omega\mu_0(\epsilon_0 - j\sigma_d/\omega)}$ and a is the radius of the drill string. J_0 and J_1 are the zero- and first-order Bessel functions, respectively. The incident electric field $\mathbf{E}^i(\mathbf{r})$ is a voltage/current gap source, as shown in Fig. 1. The scattering electric field $\mathbf{E}^s(\mathbf{r})$ can be expressed in terms of vector potential $\mathbf{A}(\mathbf{r})$ and scalar potential $\Phi(\mathbf{r})$ through the following equation:

$$\mathbf{E}^s(\mathbf{r}) = -j\omega\mathbf{A}(\mathbf{r}) - \nabla\Phi(\mathbf{r}) \tag{3}$$

where $\omega = 2\pi f$ and f is the frequency of the source.

First, consider the case where the background formation is homogeneous isotropic media with the wavenumber

$$k = \omega\sqrt{\varepsilon_0\varepsilon_{rc}\cdot\mu_0\mu_r} \tag{4}$$

and

$$\varepsilon_{rc} = \varepsilon_r - j\frac{\sigma}{\omega\varepsilon_0} \tag{5}$$

where ε_0, ε_r, ε_{rc} σ, μ_0, and μ_r denote the permittivity of free space, the relative permittivity of the media, the relative effective permittivity of the media, the conductivity of the media, the permeability of free space, and the relative permeability of the media, respectively.

The EMT system uses very low operation frequency, from a fraction of a hertz to tens of hertz, otherwise the surface signal will be not detectable due to the heavy attenuation of electromagnetic fields passing through the formation. Hence, the drill string has an electrically small radius compared to the wavelength of the formation. So that it can be treated using the thin wire approximation that assumes the current density on the thin wire has no azimuthal component. The axially directed current on the thin wire also has no variation along the azimuthal angle. There is no radial component since the current only flows on the surface of the drill string. Accordingly, the induced surface current on the wire (drill string) is assumed to be axially directed and has no azimuthal variation [13]. Furthermore, the potentials can be represented as functions of the total induced axial current $\mathbf{I}(\mathbf{r})$ on S, i.e.,

$$\mathbf{A}(\mathbf{r}) = \mu_0\mu_r\int_S G(\mathbf{r},\mathbf{r}')\cdot\frac{\mathbf{I}(\mathbf{r}')}{2\pi a(\mathbf{r}')}dS' \tag{6}$$

and

$$\Phi(\mathbf{r}) = -\frac{1}{j\omega\varepsilon_0\varepsilon_{rc}}\int_S G(\mathbf{r},\mathbf{r}')\nabla'_S\cdot\left(\frac{\mathbf{I}(\mathbf{r}')}{2\pi a(\mathbf{r}')}\right)dS' \tag{7}$$

where $a(\mathbf{r}')$ is the radius of the drill string cross section, which includes the point $\mathbf{r}'$ on the wire axis. Here, the prime symbols denote the position of the source point. In the previously mentioned IEs

$$G(\mathbf{r},\mathbf{r}') = \frac{e^{-jkR}}{4\pi R},\ R = |\mathbf{r} - (\mathbf{r}' + \mathbf{a}(\mathbf{r}'))\,| \tag{8}$$

is Green's function for homogeneous isotropic media. The vector $(\mathbf{r}' + \mathbf{a}(\mathbf{r}'))$ is a point on the surface S, where $\mathbf{a}(\mathbf{r}')$ is a vector with magnitude of $a(\mathbf{r}')$ and points from $\mathbf{r}'$ to the surface of the drill string.

Since the current on the surface of drill string has no azimuthal variation, the so-called thin wire kernel [15]

$$K(\mathbf{r},\mathbf{r}') = \frac{1}{2\pi}\int_{-\pi}^{\pi} G(\mathbf{r},\mathbf{r}')d\phi' \tag{9}$$

can be extracted from the potential integrals (6) and (7). This thin wire kernel helps reduce the surface integrals into line integrals with the form

$$\int_L B(\mathbf{r}')K(\mathbf{r},\mathbf{r}')dl' \tag{10}$$

where $B(\mathbf{r}')$ is the total scalar current or charge on the circumference of the corresponding cross section and L is the axial length of the thin wire. Accurate evaluation of the thin wire kernel is vital to model the thin wire structure. The potential integrals on thin wire can be calculated with high accuracy when singularity cancellation schemes are employed. For the evaluation and integration of the thin wire kernel, refer to [15].

B. Green's Function for Layered Uniaxial Media

Now consider multilayered media with homogeneous uniaxial media for each layer, as shown in Fig. 1. For each layer, the uniaxial conductivity tensor $\boldsymbol{\sigma} = \mathcal{I}_t\sigma_t + \hat{\mathbf{z}}\hat{\mathbf{z}}\sigma_z$ is incorporated into the relative effective or complex permittivity $\boldsymbol{\varepsilon}_{cr} = \mathcal{I}_t\varepsilon_{crt} + \hat{\mathbf{z}}\hat{\mathbf{z}}\varepsilon_{crz}$ by the formulas $\varepsilon_{crt} = \varepsilon_{rt} - j\frac{\sigma_t}{\omega\varepsilon_0}$ and $\varepsilon_{crz} = \varepsilon_{rz} - j\frac{\sigma_z}{\omega\varepsilon_0}$, where $\mathcal{I}_t$ is the transverse unit dyadic, and the relative permeability of uniaxial media is $\boldsymbol{\mu}_r = \mathcal{I}_t\mu_{rt} + \hat{\mathbf{z}}\hat{\mathbf{z}}\mu_{rz}$.

The time-harmonic Maxwell's equations are

$$\nabla\times\mathbf{E} = -j\omega\mu_0\boldsymbol{\mu}_r\cdot\mathbf{H} - \mathbf{M} \tag{11}$$

and

$$\nabla\times\mathbf{H} = j\omega\varepsilon_0\boldsymbol{\varepsilon}_{cr}\cdot\mathbf{E} + \mathbf{J} \tag{12}$$

where $\mathbf{J}$ and $\mathbf{M}$ are the electric and magnetic current sources, respectively.

Because Green's function is the solution to a dipole source, it is never a trivial task to acquire the closed-form Green's function for layered uniaxial media in spatial domain. Since the formation is symmetric w.r.t. the vertical axis, we express any vector component as $\mathbf{F}(\mathbf{r}) \equiv \mathbf{F}(\boldsymbol{\rho}, z)$, where $\boldsymbol{\rho} = \hat{\mathbf{x}}x + \hat{\mathbf{y}}y$ is the projection of $\mathbf{r}$ on the xy plane. Then, we define a 2-D Fourier transformation for all the fields w.r.t. to the transverse plane to facilitate the analysis of layered uniaxial media. After the Fourier transformation, the layered media problem goes into spectral domain. The physical meaning of the Fourier transformation is to convert a dipole source in spatial domain into an infinity series of plane waves in spectral domain. The modeling of plane waves propagating in layered uniaxial media can be solved using the transmission line analogy [22].

The analogy of transmission line facilitates to obtain the MP-LMGF, which is in dyadic form [22]. For thin wire structure in layered media, the vector and scalar potentials relate to the

electric current source and LMGF via

$$\mathbf{A}(\mathbf{r}) = \mu_0 \int_S \mathcal{G}^{\mathbf{A}}(\mathbf{r},\mathbf{r}') \cdot \frac{\mathbf{I}(\mathbf{r}')}{2\pi a(\mathbf{r}')} dS' \tag{13}$$

$$\Phi(\mathbf{r}) = -\frac{1}{j\omega\varepsilon_0}\left[\int_S K^{\Phi}(\mathbf{r},\mathbf{r}')\nabla'_S \cdot \frac{\mathbf{I}(\mathbf{r}')}{2\pi a(\mathbf{r}')} dS' + \int_S P_z(\mathbf{r},\mathbf{r}')\hat{\mathbf{z}} \cdot \frac{\mathbf{I}(\mathbf{r}')}{2\pi a(\mathbf{r}')} dS'\right]. \tag{14}$$

Components of the dyadic Green's function $\mathcal{G}^{\mathbf{A}}$ physically represent the components of the magnetic vector potential at $\mathbf{r}$ for the variously oriented unit-strength electric current dipoles at $\mathbf{r}'$. K^{Φ} is the corresponding scalar potential kernel, and P_z is the vertical current scalar potential correction factor for layered media. All Green's functions are called the mixed-potential form of LMGF or MP-LMGF. Similar formulas can be acquired for magnetic dipole source. For conciseness, they are not discussed here and in the following.

These dyadic and scalar LMGFs do not have a close form in spatial domain and need to be calculated from their corresponding spectral form with the help of inverse Fourier transformation

$$\begin{bmatrix} \mathcal{G}^{\mathbf{A}} \\ K^{\Phi} \\ P_z \end{bmatrix} = \frac{1}{(2\pi)^2} \int_{-\infty}^{\infty}\int_{-\infty}^{\infty} \times \begin{bmatrix} \tilde{\mathcal{G}}^{\mathbf{A}}(\boldsymbol{k}_\rho, z, z') \\ \tilde{K}^{\Phi}(\boldsymbol{k}_\rho, z, z') \\ \tilde{P}_z(\boldsymbol{k}_\rho, z, z') \end{bmatrix} e^{-j\mathbf{k}_\rho \cdot (\boldsymbol{\rho}-\boldsymbol{\rho}')} dk_x dk_y \tag{15}$$

where the functions in the square brackets at the right-hand side are the corresponding spectral components of LMGFs that can be expressed using the analogy of transmission line voltages and currents. More distinctly, these LMGFs in the spectral domain are

$$\tilde{\mathcal{G}}^{\mathbf{A}}(\mathbf{k}_\rho, z, z') = \begin{bmatrix} \frac{1}{j\omega\mu_0} V_i^h & 0 & 0 \\ 0 & \frac{1}{j\omega\mu_0} V_i^h & 0 \\ \frac{\mu_t k_x}{jk_\rho^2}(I_i^h - I_i^e) & \frac{\mu_t k_y}{jk_\rho^2}(I_i^h - I_i^e) & \frac{\mu_t}{j\omega\varepsilon_0\varepsilon'_{cz}} I_v^e \end{bmatrix} \tag{16}$$

$$\tilde{K}^{\Phi}(\mathbf{k}_\rho, z, z') = j\omega\epsilon_0 \frac{V_i^e - V_i^h}{k_\rho^2} \tag{17}$$

and

$$\tilde{P}_z(\mathbf{k}_\rho, z, z') = \frac{k_0^2 \mu'_r}{k_\rho^2}(V_v^h - V_v^e) \tag{18}$$

where V and I are, respectively, the voltage and current on the transmission line model of the layered structure. The definitions and expressions for the voltages and currents appearing in the spectral form can be found in [22]. The unprimed material parameters in (16)–(18) are evaluated at the observation point $\mathbf{r}$, whereas the primed parameters are evaluated at the source point $\mathbf{r}'$.

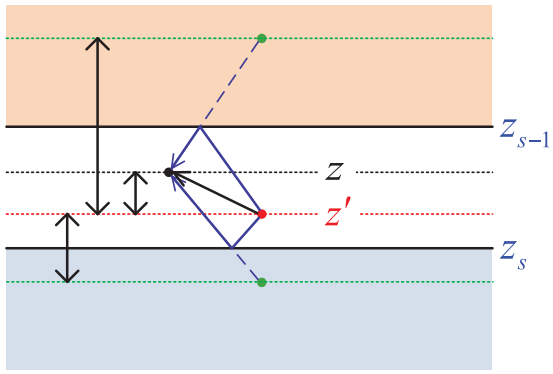

Fig. 2. Direct radiation (black line) and reflection from lower and upper boundaries (blue line) when the source point and observation point are in the same layer.

After the LMGFs are obtained in the spectral domain, we are ready to calculate the LMGFs in spatial domain using (15). To save the computation effort, Hankel transform is applied to reduce the double infinite integral into a single semi-infinite integral. With a rigorous derivation, the calculation of all the components of LMGFs involving general electric and magnetic sources can be expressed in terms of 14 independent integrals [23]. All of them are in the form of the generalized Sommerfeld integral (SI)

$$S_n\{\tilde{F}(k_\rho)\} = \frac{1}{2\pi}\int_0^{\infty} \tilde{F}(k_\rho) J_n(k_\rho|\boldsymbol{\rho}-\boldsymbol{\rho}'|) k_\rho dk_\rho. \tag{19}$$

Here, J_n is the Bessel function of the first kind of order n with $n = 0, 1, 2$ and $\boldsymbol{\rho}$, $\boldsymbol{\rho}'$ are the cylindrical coordinates of the projections of the observation and source points on the transverse plane. The algorithm for the accurate and efficient evaluation of these independent SIs involves the deformed integral path [24], acceleration and regularization of SIs by asymptotic singularity extraction [23], [25]–[27], and weighted average method for the integral tails [28], [29].

To accelerate the evaluation of the generalized SIs in (19) when small vertical displacements between source and observation points present, the asymptotic terms from the integrand can be extracted. These terms are generally interpreted as direct radiation and reflection from lower and upper boundaries of the source layer when source and observation points are in the same layer, as shown in Fig. 2. When source and observation points are in two adjacent layers, the extracted term is only the direct term. When source and observation points are separated by more than one layer, the exponential decay of the quantities along the transmission line guarantees sufficiently fast convergence of the integrals, and no extraction is required. The asymptotic singularity extraction can be generally expressed as

$$S_n\left\{\tilde{F}(k_\rho)\right\} = S_n\left\{\tilde{F}(k_\rho) - \tilde{F}^{\infty}(k_\rho)\right\} + F^{\infty}(\mathbf{r},\mathbf{r}') \tag{20}$$

with $\tilde{F}^{\infty}(k_\rho)$ being the asymptotic form of $\tilde{F}(k_\rho)$. The extracted term can be expressed by their closed form or easily evaluated

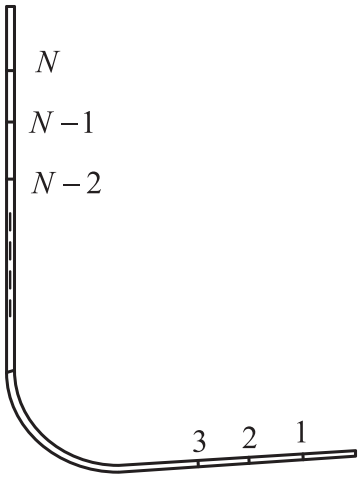

Fig. 3. Whole drill string is discretized into $(N+1)$ linear segments with N interior nodes.

form $F^{\infty}(\mathbf{r},\mathbf{r}')$ in the spatial domain with the use of the Sommerfeld and related identities, which can be found in [23].

C. Thin Wire Kernels for Layered Uniaxial Media

The spatial form of the extracted terms or $F^{\infty}(\mathbf{r},\mathbf{r}')$ is the most singular parts of the LMGFs. When these terms are extracted, all the remaining spectral difference potential kernels either vanish or are slowly varying about the drill string axis; $\mathbf{r}'$ can be a point placed on the drill string axis in (13) and (14). Thus, for layered uniaxial media, the circumferential integration and all the effects of the pipe radius are isolated to the terms containing (9) whose integrand should be modified and replaced with the asymptotic spatial form $F^{\infty}(\mathbf{r},\mathbf{r}')$, i.e.,

$$K(\mathbf{r},\mathbf{r}')=\frac{1}{2\pi}\int_{-\pi}^{\pi}F^{\infty}(\mathbf{r},\mathbf{r}')d\phi'. \tag{21}$$

We call them the thin wire kernels for layered media. Because it is nontrivial to find a singularity cancellation scheme to smooth the integrands of these thin wire kernels, we employ the Gauss–Legendre rule to calculate the corresponding thin wire kernels for LMGFs and good results are obtained.

D. Method of Moments

MoM transforms the governing equation (1) into a dense matrix equation to enable its solution by digital computers. First, the drill string is subdivided into $(N+1)$ linear segments with N interior nodes, as shown in Fig. 3. Since the unknown current vanishes at the endpoints of the thin wire, the unknown current $\mathbf{I}(\mathbf{r})$ is approximated as

$$\mathbf{I}(\mathbf{r})=\sum_{n=1}^{N}I_n\mathbf{\Lambda}_n(\mathbf{r}),\quad \mathbf{r}\in S \tag{22}$$

where I_n is the unknown current coefficient on the nth interior node and $\mathbf{\Lambda}_n$ is a vector basis function used to represent the current on the wire. The triangle basis function and linear element are used in this paper. Higher order element and basis function

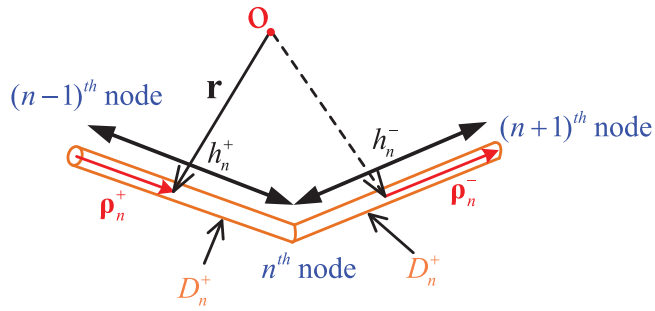

Fig. 4. Geometrical parameters associated with the nth node of wire.

can also be applied [30]. The triangle basis function is

$$\mathbf{\Lambda}_n(\mathbf{r})=\begin{cases}\dfrac{\boldsymbol{\rho}_n^+}{h_n^+}, & \mathbf{r}\in D_n^+\\ \dfrac{\boldsymbol{\rho}_n^-}{h_n^-}, & \mathbf{r}\in D_n^-\\ 0, & \text{elsewhere}\end{cases} \tag{23}$$

where, as illustrated in Fig. 4, $D_n^{\pm}$ is the $\pm$ reference segment attached to the nth nonboundary node of a wire. The length of $D_n^{\pm}$ relative to the nth node is $h_n^{\pm}$, and $\boldsymbol{\rho}_n^{\pm}$ is $(\pm)\times$ (the vector from the free node to $\mathbf{r}$). Inserting (3), (13), (14), and (22) into (1), and applying the Galerkin form of the MoM, we obtain

$$\{[Z_{mn}]+[Z_I]\}[I_n]=[V_m^i] \tag{24}$$

where $[Z_{mn}]$ represents the mutual impedance between nodes m and n, $[Z_I]$ is the matrix corresponding to the internal impedance of the drill string, and $[V_m^i]$ corresponds to the impressed voltage at the gap source. The evaluations of the $[Z_{mn}]$, $[Z_I]$, and $[V_m^i]$ are

$$Z_{mn}=\langle\mathbf{\Lambda}_m;j\omega\mathbf{A}(\mathbf{\Lambda}_n)\rangle_{D_m}+\langle\mathbf{\Lambda}_m;\nabla\Phi(\mathbf{\Lambda}_n)\rangle_{D_m} \tag{25}$$

$$Z_I=Z_i\langle\mathbf{\Lambda}_m;\mathbf{\Lambda}_n\rangle_{D_m} \tag{26}$$

$$V_m=\langle\mathbf{\Lambda}_m;\mathbf{E}^i(\mathbf{r})\rangle_{D_m} \tag{27}$$

where

$$\langle\mathbf{X};\mathbf{Y}\rangle_{D_m}=\int_{D_m^+ + D_m^-}\mathbf{X}\cdot\mathbf{Y}\,dl \tag{28}$$

and $\mathbf{A}(\mathbf{\Lambda}_n)$ and $\Phi(\mathbf{\Lambda}_n)$ can be evaluated by (13) and (14).

The entries of the system matrix and vector can be evaluated using the method proposed for thin wire model in [15]. Once the current distribution on the drill string is solved out, it is easy to calculate the electromagnetic field at any position using (3) and to obtain the voltage drop received by a surface receiver.

E. Modeling of the Drilling Fluid

The drill string is usually surrounded by drilling fluid that can be composed of water, oil, and gas. Different drilling fluid has different electric conductivity. It is interesting to investigate the influence of the fluid to the EMT system. Assuming that the drill string is in the center of the borehole, Fig. 5 shows the cross section of the borehole with drill string and drilling fluid inside. The radius of the drill string is a and the outer radius of the

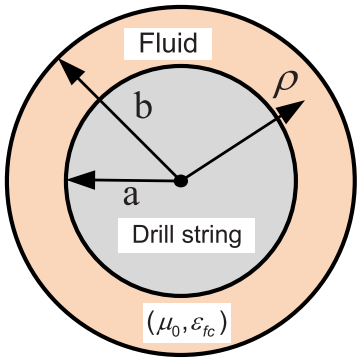

Fig. 5. Cross section of the borehole with drill string placed in the center and drilling fluid.

drilling fluid is b. The permeability and effective permittivity of the drilling fluid are denoted by $(\mu_0, \varepsilon_{fc})$. Applying the theory of volumetric equivalence principle (VEP), we can model the drilling fluid as equivalent volume current

$$\mathbf{J}_v(\mathbf{r}) = j\omega(\varepsilon_{fc} - \varepsilon_b)\mathbf{E}(\mathbf{r}) \tag{29}$$

where ε_b is the effective permittivity of the background formation. Then, the electric field inside the drilling fluid can be acquired using the current continuity equation and the quasi-static approximation since the working frequency of the EMT system is low. Using the equation of continuity, the charge density on the surface of the drill string is related to the surface current by

$$q_s = -\frac{1}{j\omega 2\pi a}\frac{dI(l)}{dl}. \tag{30}$$

For a perfectly conducting wire, the ρ component of the electric flux density D_ρ at the surface of the wire, is equal to q_s. The electric field on the surface of the uncoated wire then is approximated by

$$\mathbf{E}(\rho = a) = \hat{\boldsymbol{\rho}}\frac{q_s}{\varepsilon_{fc}} = -\hat{\boldsymbol{\rho}}\frac{1}{j\omega 2\pi a\varepsilon_{fc}}\frac{dI(l)}{dl}. \tag{31}$$

The tangential component of the electric field inside the fluid or borehole is considered to be negligible. To extrapolate from the value at the wire surface to points in the drilling fluid, we assume a $\frac{1}{\rho}$ radial variation, which is appropriate for quasi-static approximation. Then, this electric field in the fluid can be expressed as

$$\mathbf{E}(\rho) = -\hat{\boldsymbol{\rho}}\frac{1}{j\omega 2\pi\rho\varepsilon_{fc}}\frac{dI(l)}{dl},\ a \le \rho \le b \tag{32}$$

which is inversely proportional to the radial distance ρ and is radial directed. The quasi-static property confines the equivalent charges to the surface of the drill string and the outer boundary of the drilling fluid, since the current has zero divergence except for the discontinuities at the inner and outer boundaries. Combining (29) and (32), we can get the expression of the volumetric equivalent currents and equivalent charges using only the axial current $\mathbf{I}(\mathbf{r})$ on the drill string. Hence, the modeling of the drilling fluid does not increase the number of unknowns.

Compared with the volume-surface integral equation (VSIE) approach for scattering from composite conducting-dielectric objects [31], [32], our approach only needs to solve the EFIE, not the combination of EFIE and the volume integral equation (VIE) in VSIE approach, since the volume equivalent current can be expressed by the axial current on the drill string. The only added calculations are

$$\mathbf{A}(\mathbf{r}) = \mu_0 \int_V \mathcal{G}^{\mathbf{A}}(\mathbf{r}, \mathbf{r}')\cdot \mathbf{J}_v\, dV' \tag{33}$$

$$\Phi(\mathbf{r}) = -\frac{1}{j\omega\varepsilon_0}\left[\int_V K^{\Phi}(\mathbf{r}, \mathbf{r}')\nabla'_S\cdot\mathbf{J}_v\, dV' + \int_V P_z(\mathbf{r}, \mathbf{r}')\hat{\mathbf{z}}\cdot\mathbf{J}_v\, dV'\right] \tag{34}$$

the volume integrals of the volume equivalent current and its divergence. For details of the volume integral, refer to [33] and [34], and no more details will be discussed.

III. Numerical Examples and Discussion

Based on the derivation, we implemented the modeling algorithms to solve the current distribution on the drill string and compute the excited electric field by the voltage/current gap source. One should note that the current distribution induced by one current gap source can be acquired by normalizing the current distribution induced by a voltage gap source. Both vertical and horizontal wells in layered uniaxial media are simulated to validate our method. Further simulations and results are discussed to illustrate the flexibility of our method to model various EMT systems. In all the simulations, the conductivity of air is taken as 10^{-6} S/m, and the relative permittivity and permeability of the layered formation are both one.

A. Validation

First, to validate the proposed method, a vertical well in layered uniaxial media is studied. The formation has three layers excluding the half-space filled with air on the top. The horizontal conductivity in each layer is, from top to bottom, 0.5, 0.1, and 0.05 S/m, respectively. And the vertical conductivity in each layer is, from top to bottom, 0.1, 0.02, 0.01 S/m, respectively. The interfaces are at $z = 400$ m and $z = 700$ m. The 1000-m-long vertical drill string has a radius of 12.7 cm. A 1-A current source is placed at depth $z = 960$ m and it works at 5 Hz. Fig. 6 shows the magnitude and phase of the axial current distributions on the vertical drill string when the drill pipe is PEC and has a conductivity of 10^5 S/m. The results obtained by the commercial FEM software COMSOL and the proposed method agree very well both in the magnitude and phase of the axial current. And from the results, we observe that the current decays faster inside layer with higher conductivity. This is reasonable because more current will leak into the more conductive formation resulting larger attenuation of the current on the drill string. Moreover, conductivity of the drill string also influences the attenuation rate of the current. As shown in the results, it is clear that the

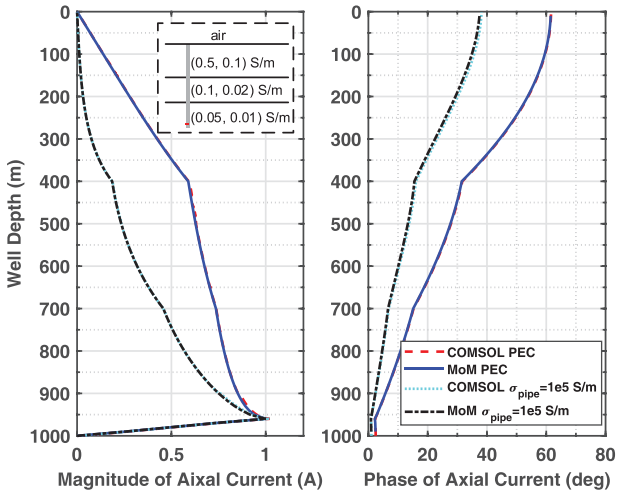

Fig. 6. Magnitude (left-hand side) and phase (right-hand side) of the axial current on the 1000-m-long vertical well in three-layer uniaxial media.

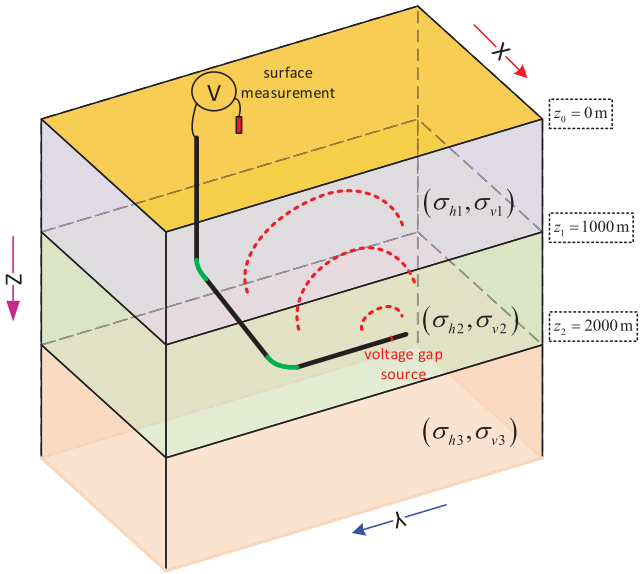

Fig. 7. Well with complicate 3-D trajectory in three-layer uniaxial media.

lower the conductivity of the drill string is, the faster the current along the well decays.

The cases studied up to now are limited to the vertical well. Hence, a more convincing case that has complicate well trajectory in layered uniaxial media will be studied to demonstrate the efficiency and accuracy of our method. The 3-D trajectory of the well and the layered uniaxial media is shown in Fig. 7. The uniaxial conductivity of layer i $(i = 1, 2, 3)$ is denoted by $(\sigma_{hi}, \sigma_{vi})$, where σ_{hi} and σ_{vi} denote the horizontal conductivity and the vertical conductivity, respectively. The interfaces are $z = 0, 1000, 2000$ m and $(\sigma_{h1}, \sigma_{v1}) = (0.5, 0.5)$ S/m, $(\sigma_{h2}, \sigma_{v2}) = (0.1, 0.02)$ S/m, $(\sigma_{h3}, \sigma_{v3}) = (0.05, 0.05)$ S/m. The conductivity of air is assumed to be 10^{-6} S/m. The 3-D trajectory of the well composes of five parts among which three of them are straight lines and two of them are arcs. Three straight lines (black lines) shown in Fig. 7 can be expressed as (from top to bottom)

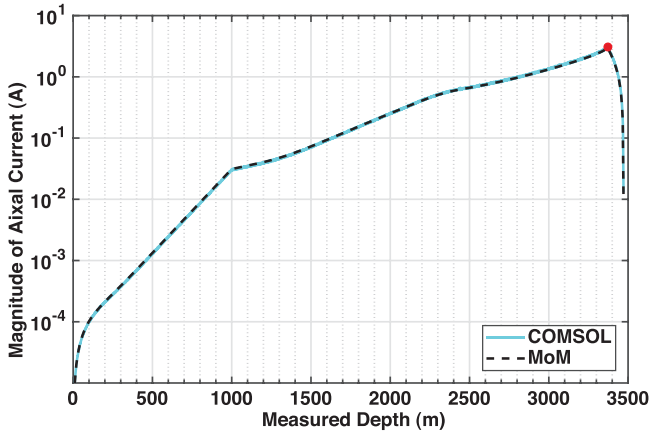

Fig. 8. Current distribution on the drill string for the complicate well inside a layered formation shown in Fig. 7.

$$\begin{cases} x = 0 \\ y = 0 \\ z = 1000 \times t \end{cases} \qquad t \in [0, 1) \tag{35}$$

$$\begin{cases} x = 200 - 100\sqrt{2} + 500\sqrt{2} \times t \\ y = 0 \\ z = 1000 + 100\sqrt{2} + 500\sqrt{2} \times t \end{cases} \qquad t \in [0, 1) \tag{36}$$

and

$$\begin{cases} x = 200 + 500\sqrt{2} \\ y = -200 - 1000 \times t \\ z = 1000 + 700\sqrt{2} \end{cases} \qquad t \in [0, 1] \tag{37}$$

respectively. Meanwhile, two arcs (green curves) connect the straight lines with a large radius of 200 m and the radians of the two arcs are 45° and 90°, as shown in Fig. 7. Hence, the whole well composes a vertical part, a deviated part, and a horizontal part. A 1-V voltage gap source is located at 100 m away from the head of the well. The total length of the well is 3471.24 m. It is assumed that the drill string is PEC.

In Fig. 8, the magnitude of the axial current along the 3-D well is shown in log scale when the EMT system employs the 1-V voltage source and works at 20 Hz. Measured depth represents the length along the trajectory of the drill string. As shown in the figure, the results obtained by the COMSOL and the proposed method match very well and the current reaches its peak value at the position of the voltage gap source. Meanwhile, from Fig. 8, one can observe that even though the deviated part (the middle black line in Fig. 7) and the horizontal part (the bottom black line in Fig. 7) of the well are in the same layer, the rates of the attenuation of the current magnitude on them are different. The attenuation rate of the current from 3300 to 2500 m (horizontal part) is smaller than that from 2200 to 1200 m (deviated part). Obviously, the reason for this discrepancy is that the vertical conductivity in that formation layer is one fifth of the horizontal conductivity. Comparing the computation cost of COMSOL and

TABLE I
COMPUTATION COST FOR 3-D CASE

	memory cost	CPU time
COMSOL	497 GB	256 minutes
this method	6.5 MB	39 seconds

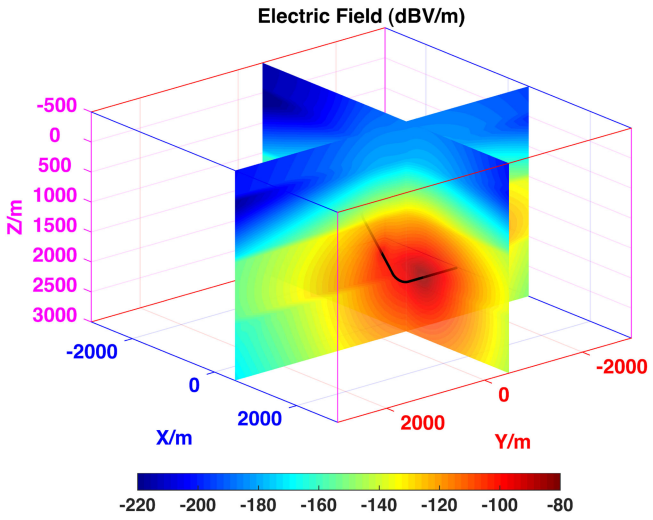

Fig. 9. Magnitude of the total electric field of two vertical slices for the EMT system shown in Fig. 7. Black curve represents the well trajectory.

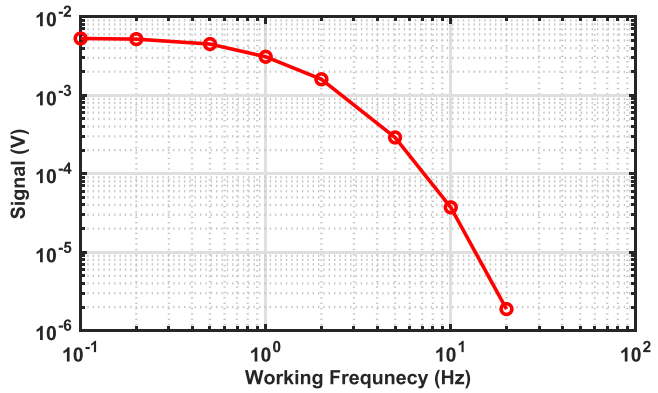

Fig. 10. Magnitude of the received signal at surface versus the working frequency.

the proposed method as listed in Table I, the proposed method is much more efficient to model the complicated well in layered uniaxial media. Fig. 9 shows two slices of the total electric field in the formation and air. The trajectory of the 3-D well is also plotted as black curve to give a better illustration. While the transverse component electric field is continuous at the interface, the normal component is not. As a result, a clear pattern of layered structure can be observed from the discontinuous fields at the interfaces. More interestingly, because the drill string extends on a large scale in the second layer, the electric field in the second layer having high conductivity attenuates more slowly than the bottom layer having low conductivity. To study the behavior of this EMT system for the specific layered formation versus working frequency, Fig. 10 shows the reduction of the

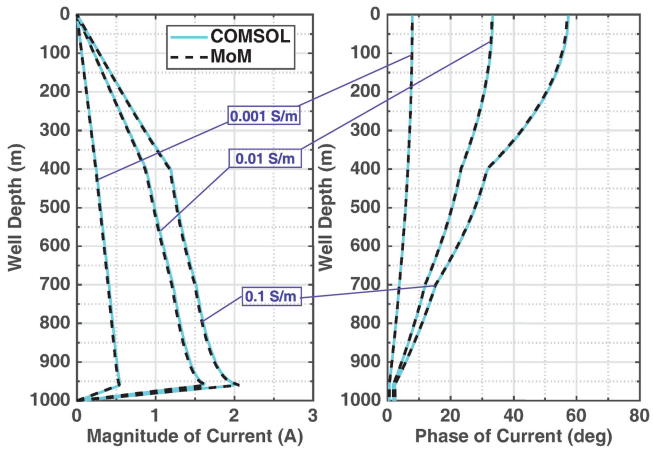

Fig. 11. Magnitude (left-hand side) and phase (right-hand side) of the axial current distributions on the drill string when drilling fluid is of different conductivity. The radius of the borehole is 17.8 cm.

magnitude of the received signal by the surface antenna when the working frequency goes high. The surface antenna links the wellhead and a point in the $-y$ direction that is 100 m away from the wellhead. As the frequency is below 1 Hz, no significant change of the signal is observed. However, the signal decreases quickly and will go indistinguishable from the environmental noise when the frequency of the source is above 10 Hz.

B. *Effect of the Drilling Fluid*

The effect of the drilling fluid can be modeled by applying the equivalence principle. The various types of drilling fluid fall into a few broad categories, such as water-based mud and oil-based mud. The effects of drilling fluid to the EMT signal, under some circumstances, are not negligible and must be taken into consideration.

Inserted into the same layered uniaxial media as depicted in Fig. 6, the 1000-m-long vertical well is in the center of a borehole whose radius is 5.0 cm larger than the drill string, i.e., 17.8 cm. A 1-V voltage gap source is embedded at $z = 960$ m depth and its frequency is 5 Hz. Fig. 11 shows the axial current distributions on the drill string when the conductivity of the drilling fluid changes from 0.001 to 0.1 S/m, corresponding to changing from oil-based mud to water-based mud. The results obtained by our method closely match with the results obtained from COMSOL. As shown in the results of Fig. 11, compared with water-based mud, the oil-based mud reduces the strength and maximum of the current on the drill string substantially, thus leading to weaker signal received by the surface antenna. The oil-based mud raises the total resistivity of the formation and leads to a smaller axial current when constant voltage source is employed. We should point out that, if the gap source is a constant current source, the conclusion will be opposite, arriving at one that the current on the drill string attenuates faster in water-based mud compared with oil-based mud.

Our method for the modeling of the drilling fluid can be further validated by an extreme case. We keep the same drill string and layered media as the case in Fig. 11, but now the borehole

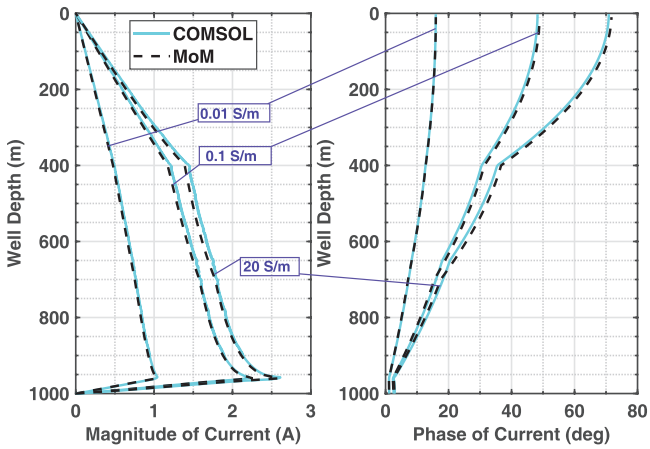

Fig. 12. Magnitude (left-hand side) and phase (right-hand side) of the axial current distributions on the drill string when drilling fluid is of different conductivity. The radius of the borehole is 50.8 cm.

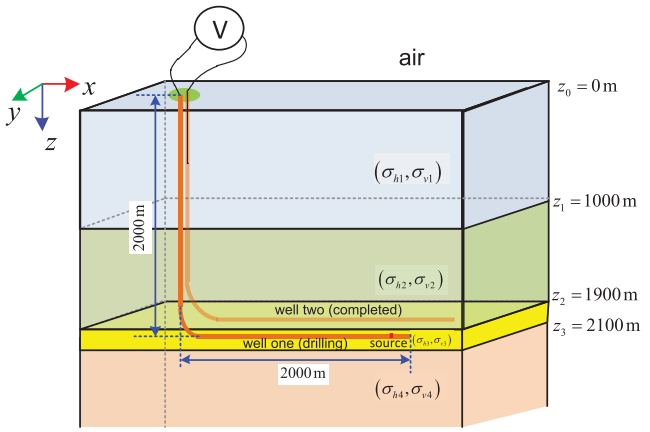

Fig. 13. Crosswell EM telemetry system. Well 1 is being drilled, whereas well 2 is completed and cased.

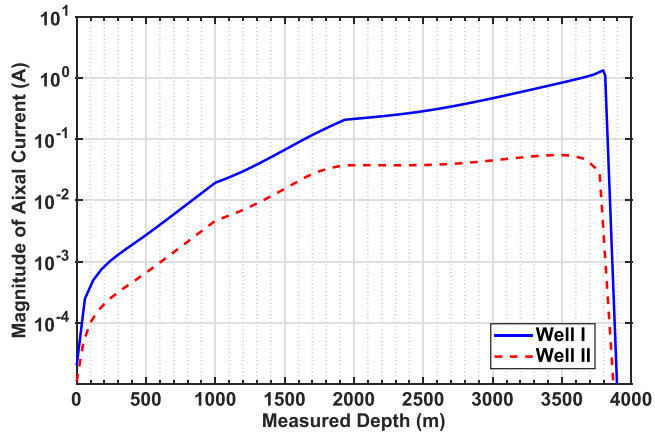

Fig. 14. Current distribution on the two horizontal wells shown in Fig. 13.

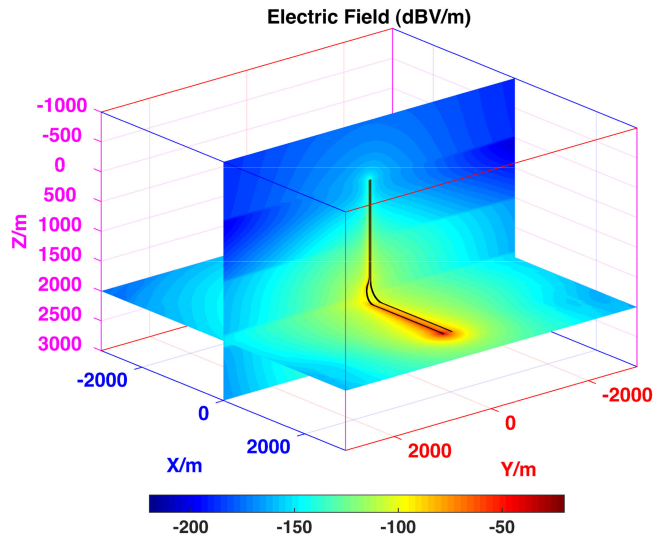

Fig. 15. Magnitude of the total electric field of two slides for the crosswell EMT system shown in Fig. 13.

radius is 50.8 cm that is uncommon in realistic situations and the mud conductivities are higher. Fig. 12 shows the axial current distributions on the drill string when the conductivity of the drilling fluid changes from 0.01 to 20 S/m. Even under such an extreme situation, the results calculated by our method agree closely with the results calculated by COMSOL.

C. Crosswell EM Telemetry System

The traditional EMT system deploys the receiver antenna at the surface where the electromagnetic field is very small compared with the field in the formation. To enhance the strength of the received signal, the technology of the crosswell EMT system [35], which is available at low cost in pad drilling, begins to be employed in practice. The main idea of the crosswell EMT system is to use the casing of a nearby completed well as an electrode that inserts into the deep formation. This deep electrode can enhance the strength of the received signal by several orders of magnitude compared to the traditional EMT system. Fig. 13 shows a crosswell EMT system in a four-layer formation. The uniaxial conductivities of the four layers are $(\sigma_{h1}, \sigma_{v1}) = (0.2, 0.2)$ S/m, $(\sigma_{h2}, \sigma_{v2}) = (0.1, 0.025)$ S/m, $(\sigma_{h3}, \sigma_{v3}) = (0.02, 0.01)$ S/m, and $(\sigma_{h4}, \sigma_{v4}) = (0.05, 0.05)$ S/m, respectively. The thin reservoir is located between $z = 1900$ m and $z = 2100$ m planes. Two horizontal wells are drilled from a single, compact piece of land known as pad, to land into the reservoir layer at depth $z = 2000$ m parallelly with a horizontal separation of 167.6 m. Both wells last until reaching a horizontal length of 2000 m. The distance between the vertical parts of the two wells is 30 m. The curvature of the curved part of both wells is 300 m although well 1 stays inside $y = 0$ m plane, whereas well 2 is not. See Fig. 15 for better illustration. Well 2 is completed and cased with conductive casing along the whole path. When well 1 is being drilled, the crosswell EMT system deploys a cable that connects to one point on the casing of well 2 and detects the voltage drop between that point and the wellhead of well 1. The drill string of well 1 has a radius of 0.127 m, and the casing of well 2 assumes to be uniform and have a radius of 0.254 m. The drill string of well 1 has conductivity of 10^6 S/m and the casing of well 2 has conductivity of 10^5 S/m.

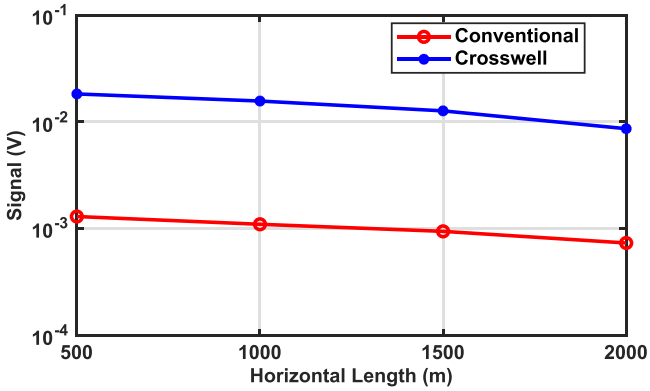

Fig. 16. Comparison of received signals by conventional and crosswell EMT systems.

In the crosswell EMT system, the 1-V voltage gap source is embedded into well 1 and has a distance of 100 m away from the drill bit of well 1. Meanwhile, it works at 20 Hz. Fig. 14 shows the current distribution on well 1 as well as the induced current on well 2. Since well 2 is a little farther away from the source, the magnitude of current on well 2 is about one order lower than that of well 1. Distinct differences between the attenuation speed of current magnitude in different layers are observed for both wells. Meanwhile, Fig. 15 shows the electric fields on one vertical slice ($y = 0$ m) and one horizontal slice ($z = 2000$ m) inside the layered formation. The trajectory of two horizontal wells are also plotted to give a better illustration. The electric field is strongest near the voltage source and then attenuates far away from the source and along the wells. Interfaces between the layers can be discerned easily from the pattern of the field. To demonstrate the advantage of the crosswell EMT system for pad drilling, the behavior of the strength of the received signal for conventional EMT system and crosswell EMT system is compared in Fig. 16. For conventional EMT system, the surface antenna detects the voltage drop between the wellhead of well 1 and one surface point 100 m away from the wellhead on the surface. While for crosswell EMT system, the deployed cable inside well 2 connects to the casing at depth of 600 m. When well 1 is being drilled from the trajectory having horizontal length of 500 m to one having horizontal length of 2000 m, the detected signal of the crosswell EMT system is about one order larger than that of the conventional EMT system.

IV. Conclusion

We have developed an efficient modeling based on EFIE, the thin wire kernel, and the MP-LMGF for the EMT system for directional drilling in layered uniaxial media. In the framework of this multiscale modeling, the dyadic and scalar representations of the LMGFs derived from transmission line analogy and SIs help calculate the electromagnetic field by arbitrarily oriented electric dipole in layered uniaxial media that is crucial to model deviated and horizontal drill string in layered media. The scheme of VEP makes it possible to quantify the influence of the thin coated drilling fluid to the EMT system. Numerical results validated and demonstrated the accuracy and efficiency of the modeling method as well as extended the method into the crosswell EMT system. The proposed method greatly relieves the modeling of arbitrary drill string in layered uniaxial media. Also, the fast modeling method makes it possible for real-time application in practice.

References

[1] "Trends in U.S. oil and natural gas upstream costs," U.S. Energy Inf. Admin., Washington, DC, USA, Tech. Rep. 2016.
[2] D. B. Bennion, F. B. Thomas, R. F. Bietz, and D. W. Bennion, "Underbalanced drilling, praises and perils," in *Proc. Permian Basin Oil Gas Recovery Conf.*, 1996, pp. 753–772.
[3] J. Chen, S. Li, C. MacMillan, G. Cortes, and D. Wood, "Long range electromagnetic telemetry using an innovative casing antenna system," in *Proc. SPE Annu. Tech. Conf. Exhib.*, 2015, pp. 1–10.
[4] D. A. Hill and J. R. Wait, "Electromagnetic basis of drill-rod telemetry," *Electron. Lett.*, vol. 14, no. 17, pp. 532–533, Aug. 1978.
[5] J. Bhagwan and F. N. Trofimenkoff, "Electric drill stem telemetry," *IEEE Trans. Geosci. Remote Sens.*, vol. GE-20, no. 2, pp. 193–197, Apr. 1982.
[6] P. DeGauque and R. Grudzinski, "Propagation of electromagnetic waves along a drillstring of finite conductivity," *SPE Drilling Eng.*, vol. 2, no. 2, pp. 127–134, Jun. 1987.
[7] M. Y. Xia and Z. Y. Chen, "Attenuation predictions at extremely low frequencies for measurement-while-drilling electromagnetic telemetry system," *IEEE Trans. Geosci. Remote Sens.*, vol. 31, no. 6, pp. 1222–1228, Nov. 1993.
[8] F. N. Trofimenkoff, M. Segal, A. Klassen, and J. W. Haslett, "Characterization of EM downhole-to-surface communication links," *IEEE Trans. Geosci. Remote Sens.*, vol. 38, no. 6, pp. 2539–2548, Nov. 2000.
[9] W. Yang, C. Torres-Verdn, J. Hou, and Z. I. Zhang, "1D subsurface electromagnetic fields excited by energized steel casing," *Geophysics*, vol. 74, no. 4, pp. E159–E180, Jul. 2009.
[10] Y. Wei, "Propagation of electromagnetic signal along a metal well in an inhomogeneous medium," Ph.D. dissertation, Dept. Elect. Power Eng., Norwegian Univ. Sci. Technol., Trondheim, Norway, 2013.
[11] J. Chen, S. Zeng, Q. Dong, and Y. Huang, "Rapid simulation of electromagnetic telemetry using an axisymmetric semianalytical finite element method," *J. Appl. Geophys.*, vol. 137, pp. 49–54, Feb. 2017.
[12] W. Li, Z. Nie, X. Sun, and Y. Chen, "Numerical modeling for excitation and coupling transmission of near field around the metal drilling pipe in lossy formation," *IEEE Trans. Geosci. Remote Sens.*, vol. 52, no. 7, pp. 3862–3871, Jul. 2014.
[13] A. F. Peterson, S. L. Ray, and R. Mittra, *Computational Methods for Electromagnetics*. New York, NY, USA: IEEE Press, 1998.
[14] D. J. Hoppe, *Impedance Boundary Conditions in Electromagnetics*. Boca Raton, FL, USA: CRC Press, 1995.
[15] D. R. Wilton and N. J. Champagne, "Evaluation and integration of the thin wire kernel," *IEEE Trans. Antennas Propag.*, vol. 54, no. 4, pp. 1200–1206, Apr. 2006.
[16] R. F. Harrington and J. L. Harrington, *Field Computation by Moment Methods*, 1st ed. London, U.K.: Oxford Univ. Press, 1996.
[17] K. A. Michalski and D. Zheng, "Electromagnetic scattering and radiation by surfaces of arbitrary shape in layered media. I. Theory," *IEEE Trans. Antennas Propag.*, vol. 38, no. 3, pp. 335–344, Mar. 1990.
[18] S. Zeng, D. Li, D. R. Wilton, and J. Chen, "Efficient simulation of electromagnetic telemetry using thin wire kernel and layered media Green's function," in *Proc. IEEE Int. Symp. Antennas Propag./USNC/URSI Nat. Radio Sci. Meeting*, 2017, pp. 1359–1360.
[19] S. Zeng, D. Li, D. R. Wilton, and J. Chen, "Fast and accurate simulation of electromagnetic telemetry in deviated and horizontal drilling," *J. Petroleum Sci. Eng.*, vol. 166, pp. 242–248, 2018.
[20] Y. P. Chen, L. Jiang, Z.-G. Qian, and W. C. Chew, "An augmented electric field integral equation for layered medium Green's function," *IEEE Trans. Antennas Propag.*, vol. 59, no. 3, pp. 960–968, Mar. 2011.
[21] Y. Ren, S.-W. Zhao, Y. Chen, D. Hong, and Q. H. Liu, "Simulation of low-frequency scattering from penetrable objects in layered medium by current and charge integral equations," *IEEE Trans. Geosci. Remote Sens.*, vol. 56, no. 11, pp. 6537–6546, Nov. 2018.
[22] K. A. Michalski and J. R. Mosig, "Multilayered media Green's functions in integral equation formulations," *IEEE Trans. Antennas Propag.*, vol. 45, no. 3, pp. 508–519, Mar. 1997.

[23] D. Li, D. R. Wilton, and D. R. Jackson, "Recent advances in evaluating Green's functions for multi-layered media and half-space problems," in *Proc. Comput. Electromagn. Int. Workshop*, 2017, pp. 1–2.
[24] M. Aksun and G. Dural, "Clarification of issues on the closed-form Green's functions in stratified media," *IEEE Trans. Antennas Propag.*, vol. 53, no. 11, pp. 3644–3653, Nov. 2005.
[25] N. J. Champagne, "A three-dimensional method of moments formulation for material bodies in a planar multi-layered medium," Ph.D. dissertation, Dept. Elect. Eng., Univ. Houston, Houston, TX, USA, 1996.
[26] E. Simsek, Q. H. Liu, and B. Wei, "Singularity subtraction for evaluation of Green's functions for multilayer media," *IEEE Trans. Microw. Theory Techn.*, vol. 54, no. 1, pp. 216–225, Jan. 2006.
[27] D. Li, "Efficient computation of layered medium Green's function and its application in geophysics," Ph.D. dissertation, Dept. Elect. Eng., Univ. Houston, Houston, TX, USA, 2016.
[28] K. A. Michalski, "Extrapolation methods for Sommerfeld integral tails," *IEEE Trans. Antennas Propag.*, vol. 46, no. 10, pp. 1405–1418, Oct. 1998.
[29] J. Mosig, "The weighted averages algorithm revisited," *IEEE Trans. Antennas Propag.*, vol. 60, no. 4, pp. 2011–2018, Apr. 2012.
[30] N. J. Champagne, D. R. Wilton, and J. D. Rockway, "The analysis of thin wires using higher order elements and basis functions," *IEEE Trans. Antennas Propag.*, vol. 54, no. 12, pp. 3815–3821, Dec. 2006.
[31] C. Lu and W. Chew, "A coupled surface-volume integral equation approach for the calculation of electromagnetic scattering from composite metallic and material targets," *IEEE Trans. Antennas Propag.*, vol. 48, no. 12, pp. 1866–1868, Dec. 2000.
[32] X.-C. Nie, N. Yuan, L.-W. Li, Y.-B. Gan, and T. S. Yeo, "A fast volume-surface integral equation solver for scattering from composite conducting-dielectric objects," *IEEE Trans. Antennas Propag.*, vol. 53, no. 2, pp. 818–824, Feb. 2005.
[33] D. Schaubert, D. Wilton, and A. Glisson, "A tetrahedral modeling method for electromagnetic scattering by arbitrarily shaped inhomogeneous dielectric bodies," *IEEE Trans. Antennas Propag.*, vol. AP-32, no. 1, pp. 77–85, Jan. 1984.
[34] M. A. Khayat, "Numerical modeling of thin materials in electromagnetic scattering problems," Ph.D. dissertation, Dept. Elect. Eng., Univ. Houston, Houston, TX, USA, 2003.
[35] S. Zeng, Q. Dong, and J. Chen, "A novel casing antenna system for cross-well electromagnetic telemetry in pad drilling," in *Proc. Unconventional Resour. Technol. Conf.*, Austin, TX, USA, Jul. 2017, pp. 430–435.

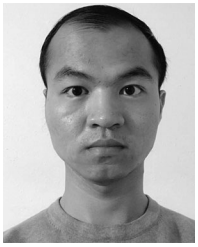

Shubin Zeng (S'17) received the B.S. degree in electrical engineering from the Huazhong University of Science and Technology, Wuhan, China, in 2013. He is currently working toward the Ph.D. degree at the Department of Electrical and Computer Engineering, University of Houston, Houston, TX, USA.

Since 2015, he has been a Research Assistant with the Department of Electrical and Computer Engineering, University of Houston. His current research interests include computational electromagnetics, subsurface characterization, and well logging.

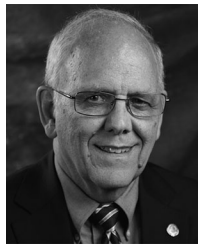

Donald R. Wilton (S'63–M'65–SM'80–F'87–LF'08) received the B.S., M.S., and Ph.D. degrees in electrical engineering from the University of Illinois at Urbana-Champaign, Champaign, IL, USA, in 1964, 1966, and 1970, respectively.

From 1965 to 1968, he was with Hughes Aircraft Company, Fullerton, CA, USA, engaged in the analysis and design of phased array antennas. From 1969 to 1970, he pursued the Ph.D. degree under a Hughes Doctoral Fellowship. From 1970 to 1983, he was with the Department of Electrical Engineering, University of Mississippi. He was a Visiting Professor with Syracuse University during the academic year 1978–1979. He was with the University of Houston from 1983 to 2012, retiring as a Professor Emeritus with the Department of Electrical and Computer Engineering. During 2004–2005 academic year, he was a Visiting Professor with the Polytechnic University of Turin, Turin, Italy, Sandia National Laboratories, and the University of Washington. His primary research focuses on computational electromagnetics, and he has authored/coauthored, lectured, and consulted extensively in this area.

Dr. Wilton was the recipient of the IEEE Third Millennium Medal. He has served the IEEE Antennas and Propagation Society as an Associate Editor for the IEEE TRANSACTIONS ON ANTENNAS AND PROPAGATION, as a Distinguished National Lecturer, and as a member of its Administrative Committee. He is also a member of Commission B of the International Radio Science Union, in which he has held various offices, including the Chair of U.S. Commission B. He was the recipient of the Applied Computational Electromagnetics Society inaugural Computational Electromagnetic Award in 2013, the IEEE Antenna and Propagation Society's inaugural Harrington-Mittra Award in Computational Electromagnetics in 2014, and the 2015 IEEE Electromagnetics Award.

Jiefu Chen (S'10–M'11) received the B.S. degree in engineering mechanics and the M.S. degree in dynamics and control from the Dalian University of Technology, Dalian, China, in 2003 and 2006, respectively, and the Ph.D. degree in electrical engineering from Duke University, Durham, NC, USA, in 2010.

He is currently an Assistant Professor with the Department of Electrical and Computer Engineering, University of Houston, Houston, TX, USA. He was a Staff Scientist with Weatherford International, Houston, TX, USA. His research interests include multiphysics modeling and inversion, computational electromagnetics and acoustics, underground and underwater wireless communication, oilfield data analytics, and well logging.